Mixed-Integer-Linear-Programming-Based Energy Management System for Hybrid PV-Wind-Battery Microgrids: Modeling, Design, and Experimental Verification

Adriana C. Luna, *Student Member, IEEE*, Nelson L. Diaz, *Student Member, IEEE*, Moisès Graells, Juan C. Vasquez, *Senior Member, IEEE*, and Josep M. Guerrero, *Fellow, IEEE*

***Abstract*—Microgrids are energy systems that aggregate distributed energy resources, loads, and power electronics devices in a stable and balanced way. They rely on energy management systems to schedule optimally the distributed energy resources. Conventionally, many scheduling problems have been solved by using complex algorithms that, even so, do not consider the operation of the distributed energy resources. This paper presents the modeling and design of a modular energy management system and its integration to a grid-connected battery-based microgrid. The scheduling model is a power generation-side strategy, defined as a general mixed-integer linear programming by taking into account two stages for proper charging of the storage units. This model is considered as a deterministic problem that aims to minimize operating costs and promote self-consumption based on 24-hour ahead forecast data. The operation of the microgrid is complemented with a supervisory control stage that compensates any mismatch between the offline scheduling process and the real time microgrid operation. The proposal has been tested experimentally in a hybrid microgrid at the Microgrid Research Laboratory, Aalborg University.**

***Index Terms*—Dispersed storage and generation, energy management, integer programming, power generation scheduling.**

I. Introduction

MICROGRIDS (MG) integrate and manage Distributed Energy Resources (DER) by ensuring a reliable and stable operation of the local energy system either when the MG is connected or disconnected to the main grid. An MG can aggregate different kinds of DERs, such as distributed generators and distributed storage, loads and power electronics devices, and grid components [1], [2]. For an interactive operation of DERs, an Energy Management System (EMS) is required to coordinate their operation within the MG [3]. The EMS provides reference profiles for the controllers of the MG in accordance to predefined objectives [4]–[6].

The energy scheduling problem for providing commands to power electronics devices has been addressed in previous works, such as [7]–[9], but only in the framework of reactive approaches (the actions are determined based on current operational conditions). On the other hand, scientific contributions focusing on the optimization problem do not consider the operation modes of the controllers and devices [2], [10], [11], or lack of experimental validation [12]. In this way, it is still missing the modeling and experimental implementation of an optimal scheduling in a microgrid that considers the demand and the availability of energy in short term, as well as the operation modes of the power electronics devices.

Several models for MG optimization have been proposed including heuristic methods such as genetic algorithms, particle swarm optimization and game theory [13]. Those methods do not guarantee the global optimal solution and may be inefficient and time-consuming [14]. Linear and dynamic programming methods ensure the optimal solution when the solution is feasible. But, they typically consider the Renewable Energy Sources (RESs) just as nondispatchable sources (input data), and, accordingly, Energy Storage Systems (ESSs) are scheduled for balancing generation and demand [2], [10], [11].

The use of ESSs in MGs demands additional technical requirements within the EMS. Especially, those based on batteries need a proper management of the State of Charge (SoC) in order to prevent fast degradation. Therefore, the ESS should be accompanied by a battery charge control which avoids overcharge and deep discharge of the battery. Meanwhile, the EMS is responsible of scheduling properly the DERs, seeking for a proper window of stored energy, and a reduction in the stress caused by repeated cycles of charge [15]. An optimal energy storage control strategy for grid-connected MGs is presented in [12], where a Mixed Integer Linear Program (MILP) opti-

Manuscript received October 28, 2015; revised January 12, 2016 and March 6, 2016; accepted June 7, 2016. Date of publication June 16, 2016; date of current version January 20, 2017. This work was supported by the Danish Energy Technology Development and Demonstration Program and also by the International Science and Technology Cooperation Program of People Republic of China through the Sino-Danish Project Microgrid Technology Research and Demonstration (meter.et.aau.dk) [24]. Recommended for publication by Associate Editor M. Molinas.

A. C. Luna, J. C. Vasquez, and J. M. Guerrero are with the Department of Energy Technology, Aalborg University, Aalborg 9220, Denmark (e-mail: acl@et.aau.dk; juq@et.aau.dk; joz@et.aau.dk).

N. L. Diaz is with the Department of Energy Technology, Aalborg University, Aalborg 9220, Denmark, and also with the Faculty of Engineering, Universidad Distrital Francisco Jose de Caldas, Bogota 110231, Colombia (e-mail: nda@et.aau.dk; nldiaza@udistrital.edu.co).

M. Graells is with the Department of Chemical Engineering, Universitat Politècnica de Catalunya, Barcelona 08036, Spain (e-mail: moises.graells@upc.edu).

Color versions of one or more of the figures in this paper are available online at http://ieeexplore.ieee.org.

Digital Object Identifier 10.1109/TPEL.2016.2581021

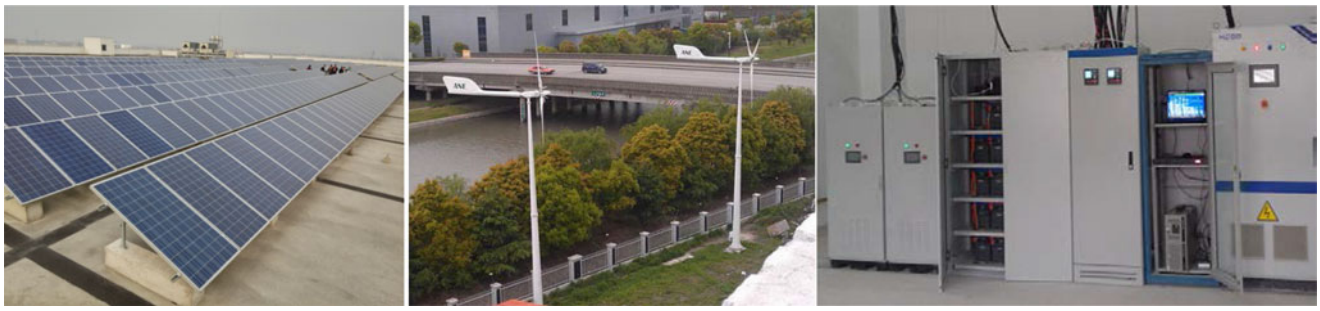

Fig. 1. Microgrid site in Shanghai.

mization is used to solve an economic problem but the results are not validated experimentally. Besides, in previous works, [12] and [16], Malysz *et al.* do not consider the fact that the ESS can get fully charged during the time horizon. In [17], an energy management strategy is proposed for operating photovoltaic (PV) power plants with ESS in order to endow them with a constant production that can be controlled. In that work, the optimization aims to keep the SoC level of the battery as close as possible to a reference value at all times. Nevertheless, keeping the SoC of batteries in a fixed level is not the best practice since battery manufacturers recommend to charge completely the batteries between discharges cycles in order to improve their performance [15]. In [18], Hooshmand *et al.* consider periods of full charge of the battery as well as reduced stress in discharge cycles of the battery by limiting the deep of discharge (DoD) to 30%. The main disadvantage of this approach is that the ESS is fully charged from the main grid at the beginning of the operation day instead of using the surplus of power from the renewable energy generators.

In the case of small-scale microgrids, the current trend is oriented to promote local consumption of the energy generated by RESs rather than exporting the surplus of electricity to the main grid [19]. This is especially important because under periods of high generation and low local consumption, the surplus of power generated from RESs and fed-in to the main grid may cause significant variations in the voltage at the common coupling point [20]. In order to ensure voltage quality in the grid-connected microgrid, the surplus in RES generation should be limited when there is not enough storage capacity in the ESSs [20]. In this sense, Ostergaard [21] defines the term *connected islanded mode* in which the MG is connected to the grid but the management is performed to avoid power exchange with the utility. One strategy to deal with this issue is by means of power curtailment of the RES generation [22]. In [23], this alternative is used to limit the power injected to the main grid. In [20], Sangwongwanich *et al.* develop a power control strategy by limiting the maximum power injected by PV systems, ensuring a smooth transition between maximum power point tracking (MPPT) mode and Constant Power Generation.

In this paper, a flexible structure of EMS for battery-based hybrid microgrids is designed and experimentally tested to provide optimal power references for DERs by considering their operation modes. The EMS includes the modeling of an optimization problem that aims to minimize operating costs, taking into account a two-stage charge procedure for ESSs based on batteries. In this way, the power delivered to the grid is limited while safe operation ranges of ESSs are ensured, which in turn, avoids their fast degradation [15]. The mathematical formulation is straightforward, reproducible and can be used and enhanced to other microgrids. The MG is complemented with the design of a fuzzy-based supervisory control level that reacts to the deviation of the utility power by adjusting the references of the DERs. This supervisory control level can also work without the EMS to provide power references in a reactive mode. The experimental verification is performed under the particular case of grid connected condition and promoting self-consumption (connected islanded mode) based on 24-h ahead prediction.

The paper is organized as follows: Section II describes the operation of the MG defined as case study, Section III includes the modeling of the optimization problem, Section IV presents the experimental results, and Section VI concludes the paper.

II. Microgrid Operation

The MG selected as case study is a lab-scale prototype of a real microgrid platform implemented in Shanghai, China (see Fig. 1) [24]. The MG consists of two RES (a wind turbine (WT) and a PV generator), each one with a power rating of 1.2 kW, a battery-based ESS, a variable load, and a critical load. The MG is connected to the main grid through a transformer as shown in Fig. 2.

Since the MG is grid-connected, the main grid imposes the conditions of the common bus (voltage and frequency) and manages any unbalance between generation and consumption. Meanwhile, DERs work as grid-following units, which are synchronized with the main grid at the connection point in order to exchange properly the power defined for each unit within the MG and with the main grid [25]. In this sense, the power references can be defined by grid noninteractive or grid-interactive operation strategies [4]. Namely, grid-noninteractive operation means that the power reference of the unit is determined locally without considering a predefined power set point (nondispatchable source). For instance, the operation of RESs, which follows MPPT algorithms or regulated charge of the ESS, can be considered as grid-noninteractive operation. On the other hand, grid-interactive operation means that the DERs will follow a power value provided by the supervisory control after adjusting the defined references given by the EMS (dispatchable source).

The supervisory control manages the deviation between the reference and measurement of the utility power due to the

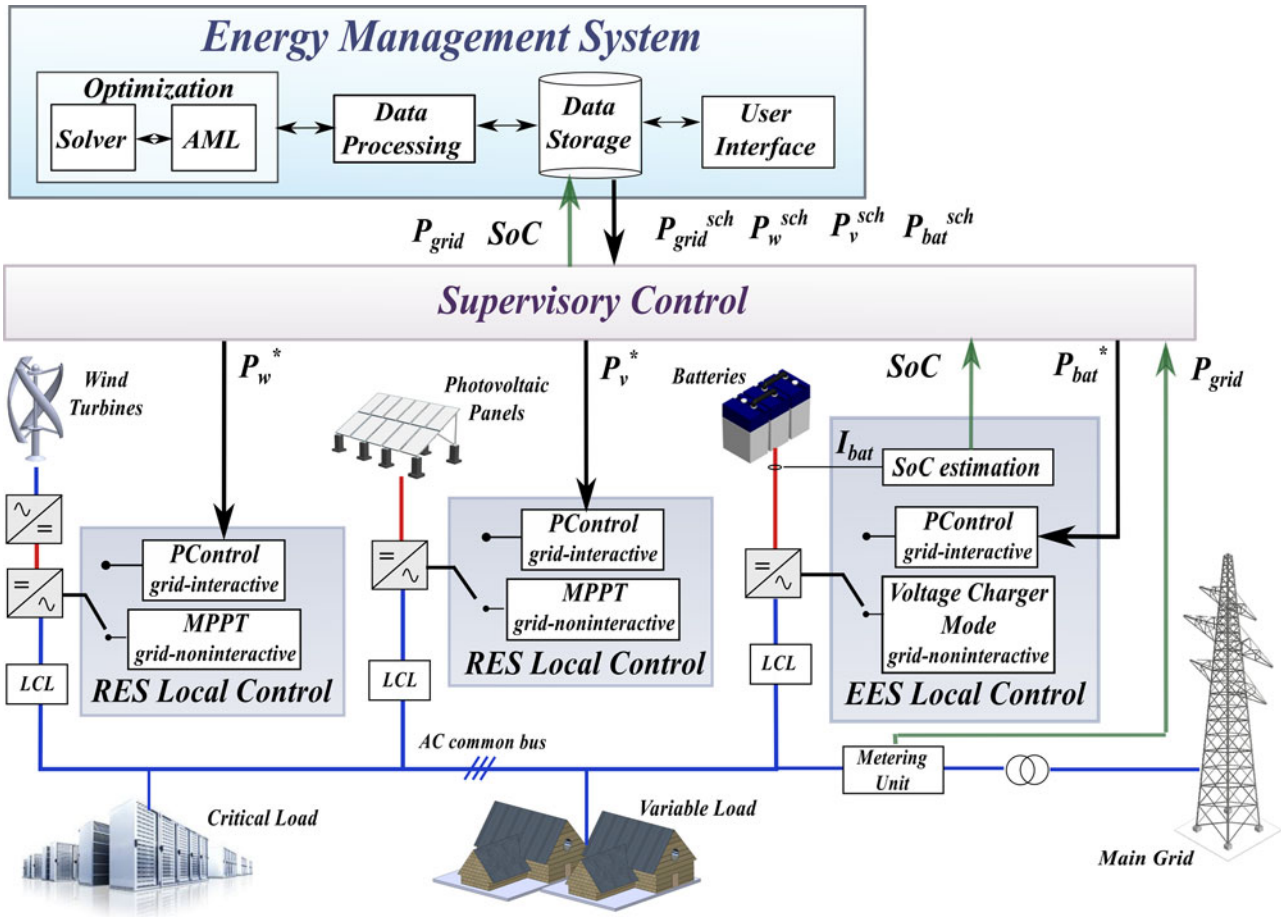

Fig. 2. Structure of the battery-based MG defined as case study.

variability and prediction errors of RESs by adapting the references of the DERs, whenever possible. The implemented strategy is based on a fuzzy inference system that adjusts the setpoints of DERs considering the SoC of the battery so that the power profiles scheduled for absorbed power from the grid can be followed.

The power references for the supervisory control are provided by the proposed EMS which is composed of four modules, *optimization*, *data processing*, *user interface*, and *data storage*. The optimization model is implemented in the module *optimization* by means of an Algebraic Modeling Language (AML) that automatically translates the problem so that the *solver* can understand it and solve the problem. The input and output data is structured by the *data processing* model and stored in the *data storage* which is a collection of files accessible by the *user interface* and the supervisory control.

A. Local Controllers

In particular, the case study considered in this paper is mainly focused on grid-connected operation of the microgrid. Because of that, the control loop of all the DERs (ESS and RES) can be unified as shown in Fig. 3, where the inner current control loop regulates the current injected or absorbed from the main grid [26]. Additionally, the current control loop is complemented with a current reference generator which generally defines the feed-forward reference signal I_{dq}^* (in d–q reference frame) as a function of the active and reactive power references P^* and Q^*, and the output voltage of each DER V_{Cdq} as

$$i_d^* = \frac{2}{3}\frac{P^*}{v_{Cd}}, \quad i_q^* = \frac{2}{3}\frac{Q^*}{v_{Cd}} \tag{1}$$

where, v_{Cd} is the d-component of V_{Cdq}, and the q-component $v_{Cq} = 0$, since each DER is synchronized with the voltage at the common coupling point V_{PCC} by means of a *phase lock loop (PLL)* [27].

For the proposed management of the microgrid, all the DERs can operate in noninteractive or grid-interactive mode in accordance to particular operational conditions of each unit. There are some differences that should be considered between the operation of the ESS and the RESs [25], [28].

1) Operation of RESs: RESs are more likely to operate by following an MPPT algorithm but, under certain conditions, it is required to limit the active power generation in accordance to optimization objectives defined by the EMS [22], [29]. Because of this, the active power reference P^* should be defined as the minimum value between the power reference established by the MPPT algorithm (P_{MPPT}) and the power reference scheduled by the EMS P^{sch}. In this way, it is possible to achieve the curtailment in the generation of RESs

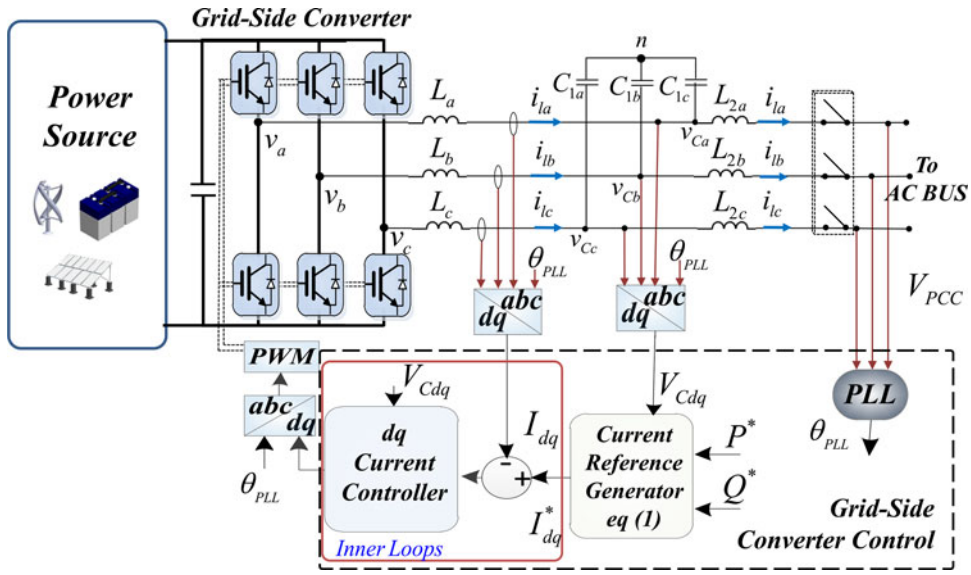

Fig. 3. Current control loop for DERs.

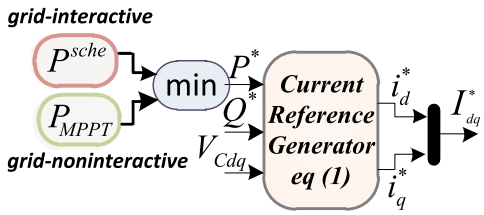

Fig. 4. Current reference generator for RESs.

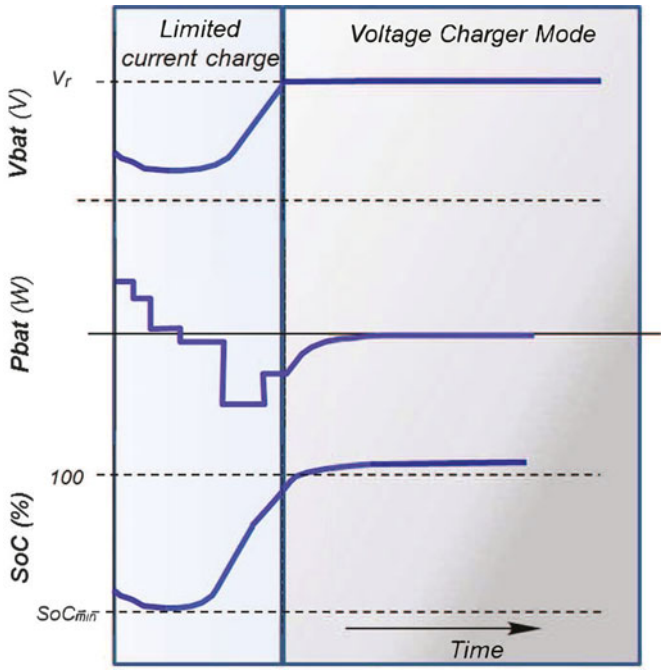

Fig. 5. Charger stage of a battery.

(grid-interactive operation) when ($P^{\mathrm{sch}} < P_{\mathrm{MPPT}}$), or ensure the maximum possible generation (noninteractive operation) in the case that ($P_{\mathrm{MPPT}} < P^{\mathrm{sch}}$). Fig. 4 shows a simplified scheme of the power reference selection for RESs where the power reference is defined as $P^* = \min(P_{\mathrm{MPPT}}, P^{\mathrm{sch}})$. It is worth to say that the MPPT algorithms are out of the scope of this paper. Interested reader may refer to [30] and [31] for MPPT strategies applied to PV and WT generators, respectively.

RESs commonly use a multistage converter in which one of them is mainly responsible of the regulation of an intermediate dc-link while the other follows the power reference. In this application, the power reference is regulated by the grid side converter (see Fig. 3) and the intermediate dc-link is assumed as regulated by the first conversion stage. Because of that, it is possible to consider RESs as a power source just as is shown in Fig. 3.

2) Operation of ESS: When the ESS is based on batteries, a two-stage charge procedure is recommended for charging them in order to limit excessive overcharge of the battery array [15], [32]. Fig. 5 represents the stages for the operation of the ESS. In the first stage (*limited current charge*), the ESS is in grid-interactive operation and injects or absorbs active power in accordance to the power reference ($P_{\mathrm{bat}}^{\mathrm{ref}}$). When the voltage per cell in the battery array reaches a threshold value V_r known as the regulation voltage (typically 2.45 ± 0.05 V/cell), the battery voltage should be limited to this value while the current at the battery approaches to zero asymptotically. In this case, the ESS switches to a grid-noninteractive operation (*voltage charger mode*) in which the ESS extracts a small amount of power from the system in order to ensure a constant voltage charge [33], [34].

The transitions of the ESS between operation modes (noninteractive and grid-interactive) are managed by a local sequential logic unit. Once the battery voltage reaches the threshold value V_r, the local unit triggers the transition between interactive to grid-noninteractive operation. Similarly, the logic unit

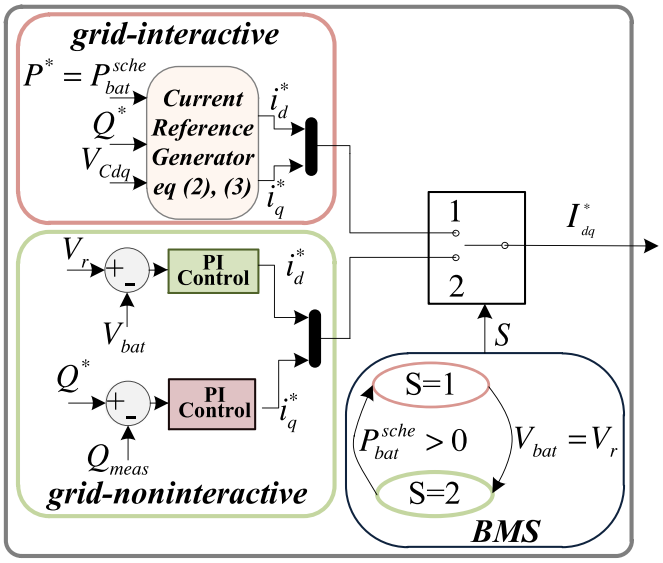

Fig. 6. Current reference generator for the ESS.

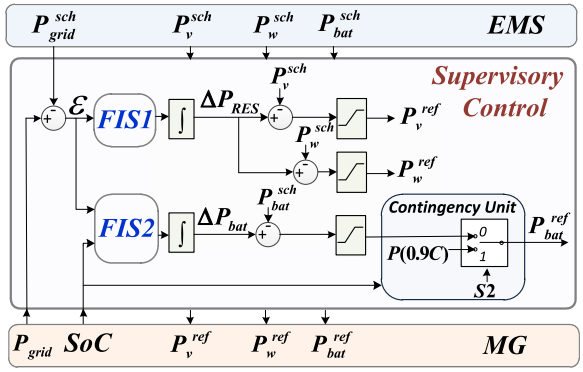

Fig. 7. Supervisory control.

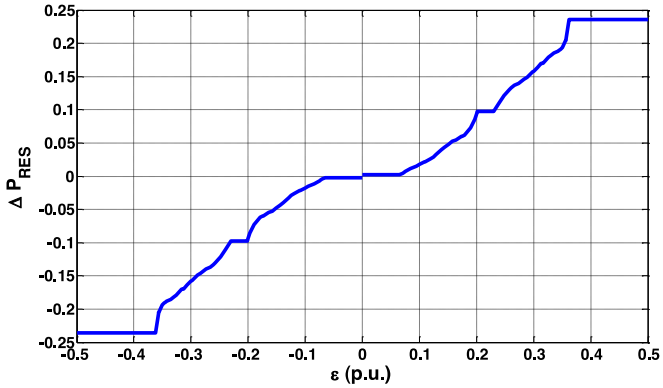

Fig. 8. Control curve for FIS1.

returns the operation of the ESS to grid-interactive operation on request ($P_{\text{bat}}^{\text{ref}} > 0$). Fig. 6 shows the current reference generation block for the ESS, including the transition table of the sequential logic unit. In the transition table, **X** indicates that the value of the variable is unimportant. The transition between operation modes depends of the current operation mode (S, where 1 represents activated state), and the logic value of the inputs ($P_{\text{bat}}^{\text{ref}} > O$ and $V_{\text{bat}} = V_r$). It is possible to see that the current reference generation under grid-noninteractive operation is quite different to the one defined previously for RESs. In order to ensure a smooth transition between operation modes, the initial conditions of inactive PI controllers are set to the active value of the reference current.

For islanded operation, one of the distributed energy resources should assume the grid-forming responsibility. Typically, the ESS assumes the regulation of the common grid, being responsible of managing the power unbalance. Therefore, for islanded operation of the microgrid the ESS should include an additional control operation mode and operates as a voltage source in voltage control mode. This mode has been previously considered in [35]. In this work, we have only considered the operation of the microgrid in grid connected operation.

B. Supervisory Control

The main idea behind supervisory control is to compensate any mismatch between the power exchanged with the main grid P_{grid} and the scheduled value obtained from the optimization process $P_{\text{grid}}^{\text{sch}}$. The core part of the supervisory control is composed of two fuzzy inference systems (FISs) with integral action. Fuzzy systems have been selected because they can synthesize easily the expected control action under different operational conditions, they can manage nonlinearities in the control action and they are straightforward to design for multivariable systems. The FISs generate incremental values ΔP_{RES} and ΔP_{bat} which are added to the scheduled values P_v^{sch}, P_w^{sch}, and $P_{\text{bat}}^{\text{sch}}$ for the RESs and the ESS, respectively, as can be seen in Fig. 7.

In Fig. 7, FIS1 represents the fuzzy inference system which generates the incremental value for RES generation (ΔP_{RES}). The input of FIS1 is the difference between P_{grid} and $P_{\text{grid}}^{\text{sch}}$

$$\mathcal{E} = P_{\text{grid}} - P_{\text{grid}}^{\text{sch}} \tag{2}$$

where positive values of $\mathcal{E}$ means that the grid is supplying more power than expected and, therefore, the power generation from the distributed units needs to be increased in order to compensate excess in the power supplied by the main grid. The output of FIS1 is integrated in order to generate the incremental value ΔP_{RES}. This value is added equally to the scheduled values of both RESs P_w^{sch} and P_v^{sch}, taking into account that the maximum generation from RESs is limited to their maximum power point value P_{MPPT}, as can be seen in Fig. 4. Fig. 8 shows the control curve for FIS1 where it is possible to see that FIS1 starts to compensate for values of $|\mathcal{E}|$ bigger than 0.05 in peer unit (the power base is 2.2 kVA).

In the case of FIS2, it is important to consider not only the value of $\mathcal{E}$ but also the SoC of the ESS. The output of FIS2 is integrated to generate the current incremental value ΔP_{bat} which is added to the scheduled value $P_{\text{bat}}^{\text{sch}}$. In this case, it is preferable to absorb some energy from the main grid rather than allow a deeper discharge of the ESS. Because of that, ΔP_{bat} is only increased when the SoC is higher than 50%, and the

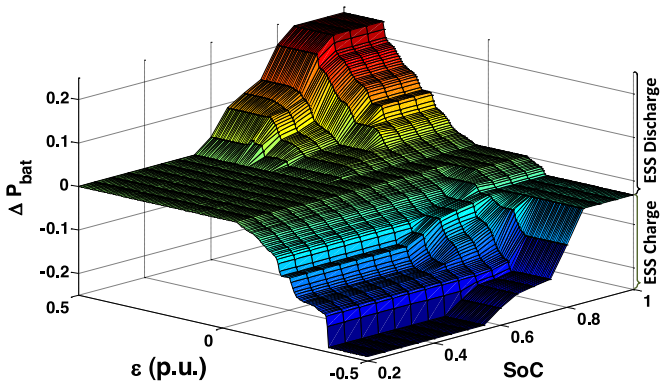

Fig. 9. Control surface for FIS2.

increment will be proportional to the current SoC and the value of $\mathcal{E}$. For negative values of $\mathcal{E}$, $\Delta P_{\rm bat}$ will decrease inversely to the SoC in order to privilege the charge of the battery for low values of the SoC rather than sending energy to the main grid. Fig. 9 shows the proposed control surface for FIS2 which shows the control action of the fuzzy system.

In this way, the supervisory control will compensate any unexpected power flow with the main grid, while it tries to avoid deeper discharge of the ESS.

The system is complemented with a contingency system for avoiding deep discharge of the ESS. This fact is particularly important by considering the uncertain behavior of the primary energy resources proposed in this case study. The contingency is activated when SoC $\leq 45\%$ and will force a limited current charge of the ESS with a charge rate of about 0.9 C where C is the battery capacity. The contingency system will be deactivated when SoC $\geq 55\%$. These values are chosen for lead acid batteries in order to keep SoC $\geq 50\%$ [15]. At this point, the supervisory control will reassure the regulation of the microgrid.

Additional functions can be included in the supervisory stage but will not be addressed in this paper to be focused on the application of the EMS. For instance, if sudden disconnection of the main grid is detected, the supervisory stage should change the operation mode of the ESS to grid-noninteractive, ensuring the power balance in the local grid. The scheduling should be executed again by setting the power of the main grid equal to 0 kW.

III. Optimization Model

In order to schedule optimal power references for the DERs in the MG, a flexible optimization problem has been defined and implemented. The model is suitable for generation-side scheduling of battery-based MGs.

A. Statements

The optimization model is presented in a generic way to be used in different structures that consider n_k ESSs, n_d dispatchable sources n_{nd} nondispatchable sources, and n_l loads. This problem is addressed as a deterministic model that relies on prediction data and by assuming that the microgrid incorporates supervisory and local controllers to manage any additional mismatch.

The model is formulated as a MILP. It includes real variables and binary variables, which are the most used type of integer variables in MILP, restricted to take values 0 or 1 [36]. This is defined in discrete time representation with t as the elementary unit in the range $t = 1, 2, ..., T$ as in [10]. Thereby, the time horizon corresponds to $T * \Delta t$. Additionally, the index k is related to ESSs and i is used for generators which, in turn, can be either i_d for dispatchable sources or i_{nd} for nondispatchable ones.

The proposed strategy aims to minimize the operating cost by setting power references for DERs. The values of active power are considered as the average in each time interval. The variables and parameters used in the mathematical formulation are summarized in Tables I and II, respectively, and will be presented during the description of the problem.

TABLE I
VARIABLES OF THE MODEL

Name	Description
Decision Variables	
$P_g^d(i_d,t)$	Power of the dispatchable source
$P_{\rm curt}(i_{nd},t)$	Curtailed power of the nondispatchable source
$P_{\rm ESS}(k,t)$	Power of the ESSs
SoC(k,t)	SoC of the ESSs
status(k,t)	Indicates if ESSs work in grid-interactive mode
Total cost	Objective function
Auxiliary Variables	
$E_g^d(i_d,t)$	Energy provided by dispatchable sources
$E_g^{nd}(i_{nd},t)$	Energy provided by nondispatchable sources
$E_{\rm ESS}(k,t)$	Energy charged/discharged by ESSs

TABLE II
PARAMETERS OF THE MODEL

Name	Description	Value
T	Number of time slots	24 (h)
Δt	Duration of interval	1 (h)
n_d	Number of disp. sources	1
n_{nd}	Number of nondisp. sources	2
n_k	Number of storage systems	1
n_l	Number of loads	2
$C(i_{nd},t)$	Cost of nondisp. sources	$[0,0]\ \forall t$ (EU)
$C(i_d,t)$	Cost of disp. sources	$2,\ \forall t \in \{6,18\} \cup$ $1,\ \forall t \notin \{6,18\}$ (EU)
$P_{g_{\max}}^d(i_d,t)$	Max power of disp. sources	0–1.2 (kW)
$P_{g_{\max}}^{nd}(i_{nd},t)$	Max pow. of nondisp. source	2 (kW)
$E_L^{\rm critical}$	Energy of the critical load	0.345 (kWh)
$E_L^{\rm variable}(t)$	Energy of the variable load	0–1 (kWh)
$P_L(t)$	Power required by the load	0.6 (kW)
$E_{\rm losses}(t)$	Average energy lost at Δt	0.072 (kWh)
$P_{\rm losses}(t)$	Power losses	0.068 (kWh)
$P_{\rm ESS_{max}}(k)$	Maximum power of ESS	1 (kW)
$P_{\rm ESS_{min}}(k)$	Minimum power of ESS	-1 (kW)
$\rm SoC_{max}(k)$	Maximum SoC	100 (%)
$SoC_{\rm min}(k)$	Minimum SoC	50 (%)
SoC$(k,0)$	Initial Condition of SoC	50–100 (%)
$\rm SoC_{th}(k)$	State of Charge threshold	96[%]
$\varphi_{\rm bat}(k)$	SOC coefficient	11.16

B. Mathematical Formulation

The problem is defined as a mixed integer linear programming, composed by real variables x, and binary variables z. The generic form to present such kind of formulations is [37],

$$\begin{aligned} \min_{x,z} \quad & f(x,z) = a^T x + b^T z \\ \text{subject to.} \quad & G(x,z) = c \\ & H(x,z) \leq d \end{aligned} \tag{3}$$

where $f(x,z)$ is the objective function presented as a linear combination of the variables, and $G(x,z)$, $H(x,z)$ are the constraints, modeled as equalities and inequalities, which are used to limit the solution in a feasible region. In turn, the objective function defines which particular assignment of feasible solution to the variables is optimal. This feasible region is convex in linear programming and, consequently, the model can ensure that the found solution is optimum related to the defined objective function [37].

Particularly, the variables used in the case study are presented in Table I. The binary variables z corresponds to status(k,t), related to the battery, and x are composed by the rest of variables. The objective function and the constraints of the optimization problem will be presented in detail through this section.

1) Objective function: The objective function has been defined to minimize operating cost, i.e., the cost for absorbing energy from the n_d generators, and it is defined as

$$\begin{aligned} f(x,z) = \ \text{Totalcost} = & \sum_{t=1}^{T} \sum_{i_d=1}^{n_d} E_g^d(i_d,t) * C(i_d,t) \\ & + \sum_{t=1}^{T} \sum_{i_{nd}=1}^{n_{nd}} E_g^{nd}(i_{nd},t) * C(i_{nd},t) \end{aligned} \tag{4}$$

where Totalcost is the value to be optimized. $E_g^d(i_d,t)$ and $E_g^{nd}(i_{nd},t)$ are the energy of the dispatchable and nondispatchable, respectively. $C(i_d,t)$ and $C(i_{nd},t)$ are the unitary cost associated to those generators.

The formulation of the objective function can be considered for several kinds of dispatchable generators. For instance, the power absorbed from the utility can be considered as a dispatchable generator, (e.g., $P_g^d(i_d,t)$, for $i_d = \{\text{utility}\}$) and the associated operating cost, $C(i_d,t)$ as a parameter that changes in terms of the time. Selling energy to the main grid can also be included in the objective function by defining an additional variable, (e.g., $P_g^d(i_d,t)$, for $i_d = \{P_{\text{sell}}\}$), with a negative value of operating cost $C(i_d,t)$, for $i_d = \{P_{\text{sell}}\}$.

Additional costs associated to DERs or distribution network are not included since this is an approach for operational level of an MG where installation, maintenance or planning costs are fixed values and do not change the optimal solution.

2) Constraints: In order to obtain a feasible optimal solution, the following constraints are defined in the optimization model as equalities and inequalities.

a) Energy balance: The energy balance must be hold all the time in the MG and can be written as

$$\begin{aligned} & \sum_{i_d=1}^{n_d} E_g^d(i_d,t) + \sum_{i_{nd}=1}^{n_{nd}} E_g^{nd}(i_{nd},t) + \sum_{k=1}^{n_k} E_{\text{ESS}}(k,t) \\ & \quad = \sum_{i_l=1}^{n_l} E_L(i_l,t) + E_{\text{losses}}(t) \ \ \forall t \end{aligned} \tag{5}$$

where $E_{\text{ESS}}(k,t)$ is the charged/discharged energy of ESSs, $E_L(i_l,t)$ is the energy required by the loads and $E_{\text{losses}}(t)$ is the energy lost in the MG.

b) Energy sources: In general, there are two types of energy sources known as dispatchable and nondispatchable sources.

The energy provided by the dispatchable sources can be defined in terms of its power as

$$E_g^d(i_d,t) = P_g^d(i_d,t) * \Delta t \ \ \forall i_d, t. \tag{6}$$

On the other hand, the recent technology of the power devices allows to manage the nondispatchable sources as dispatchable downwards, i.e., by limiting the available energy [38]. Consequently, the energy provided by these generation units can be written as

$$E_g^{nd}(i_{nd},t) = P_{g_{\max}}^{nd}(i_{nd},t) * \Delta t - P_{\text{curt}}(i_{nd},t) * \Delta t \ \ \forall i_{nd}, t. \tag{7}$$

In this case, the energy provided by these kind of sources is defined as the subtraction between the available energy of the sources and the energy scheduled to be curtailed.

c) Supplied energy: The energy requested by the loads, $E_L(i_l,t)$ is considered as a parameter, since the aim of the proposal is the generation-side scheduling in the MG.

Besides, for the sake of simplicity, the parameter $E_{\text{losses}}(t)$ is set as a constant, as presented in Table II, similar as in [39], where the losses are presented as a piecewise constant function. This value has been estimated by multiplying Δt with the average power losses obtained by means of iterative simulations in the power operation range of the DERs. It is included in the balance equation in order to compensate errors that were observed in preliminary simulations.

d) Energy storage system: The energy of the ESSs can be written in terms of their power as

$$E_{\text{ESS}}(k,t) = P_{\text{ESS}}(k,t) * \Delta t \ \ \forall k, t \tag{8}$$

where $P_{\text{ESS}}(k,t)$ is the power of the ESSs. $P_{\text{ESS}}(k,t)$ is positive when the ESS is discharged and negative when is charged.

The SoC(k,t) of each kth ESS at time t of the MG can be represented in terms of its power as

$$\begin{aligned} \text{SoC}(k,t) = \ & \text{SoC}(k,t-1) \\ & - \varphi_{\text{bat}}(k) * [P_{\text{ESS}}(k,t)\Delta t] \ \ \forall k, t \end{aligned} \tag{9}$$

where $\varphi_{\text{bat}}(k)$ is a parameter that depends on the technology of the ESS. In the algorithm, SoC$(k,t-1)$ at $t=1$, is replaced by the given initial condition SoC$(k,0)$.

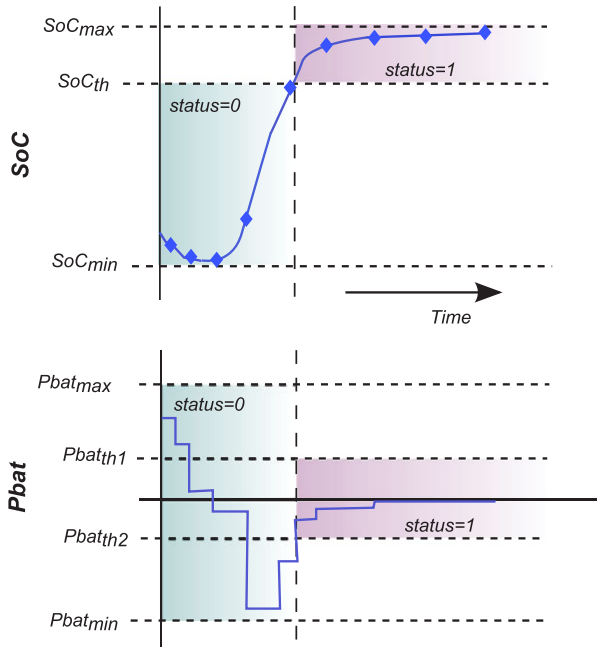

Fig. 10. Implementation of status(k,t) to consider a two-stages charger mode the kth battery.

Additionally, the global balance of the SoC is defined by establishing the condition

$$\sum_{t=1}^{T-1} \text{SoC}(k,t+1) - \text{SoC}(k,t) \geq 0 \;\; \forall k. \tag{10}$$

In this way, the SoC at the end of the time horizon is greater or equal to the initial value of SoC, ensuring similar condition for performing the scheduling of the next day.

e) Variable boundaries: The binary variable status(k,t) is included in the model to define the operation modes of the batteries, described in Section II-A2 and, accordingly, set the boundaries of the variables of the model. This variable estimates whether every kth battery is fully charged (and thus, it works in grid-noninteractive mode) or it is able to be charged/discharged (and works in grid-interactive mode) as shown in Fig. 10.

Specifically, the status(k,t) of each kth battery is equal to 1 if it is fully charged and is 0 when it can be charged/discharged, analogous to the operational modes explained in Section II-A2. The advantage of including this variable is that when the battery is charged, its power is not 0 but can be a small value. In this way, the asymptotic behavior of the grid-noninteractive operation (when the ESSs do not follow the references) can be emulated and the predicted SoC(k,t) is more accurate than in the LP model [35].

When a battery is being charged/discharged, the SoC is in the range $[\text{SoC}_{\min}, \text{SoC}_{\text{th}}]$ and the power of the battery, $Pbat = P_{\text{ESS}}$, should be in the range $[Pbat_{\min}, Pbat_{\max}]$ (see Fig. 10).

Once the SoC reaches the threshold value SoC_{th}, the battery changes its status. While the energy is enough to hold charged the battery, its SoC is set inside the region defined between SoC_{th} and $\text{SoC}_{\max}$. At the same time, the boundaries of $Pbat$ have been reduced to a narrower band $[Pbat_{\text{th1}}, Pbat_{\text{th1}}]$,

TABLE III
BOUNDARIES OF VARIABLES RELATED TO $status$

Mode	Partially Charged	Charged
status	0	1
Lowest SoC	$\text{SoC}_{\min}$	SoC_{th}
Highest SoC	SoC_{th}	$\text{SoC}_{\max}$
Lowest P_{ESS}	$P_{\text{ESS}_{\min}}$	$P_{\text{ESS}_{\text{th2}}}$
Highest P_{ESS}	$P_{\text{ESS}_{\max}}$	$P_{\text{ESS}_{\text{th1}}}$
Lowest P_g^d	0	0
Highest P_g^d	$P_{g_{\max}}^d$	0
Lowest P_{curt}	0	0
Highest P_{curt}	0	$P_{g_{\max}}^d$

instead to have a fixed maximum value, in order to emulate the asymptotic behavior of the power.

In light of the above, the boundaries of SoC(k,t) can be written at each t as

$$\begin{aligned}\text{SoC}(k,t) \leq\; & \text{SoC}_{\text{th}}(k) + (\text{SoC}_{\max}(k) \\ & - \text{SoC}_{\text{th}}(k)) * \text{status}(k,t), \quad \forall k,t \end{aligned} \tag{11}$$

$$\begin{aligned}\text{SoC}(k,t) \geq\; & \text{SoC}_{\min}(k) + (\text{SoC}_{\text{th}}(k) \\ & - \text{SoC}_{\min}(k)) * \text{status}(k,t), \quad \forall k,t. \end{aligned} \tag{12}$$

Considering the two-stage operation of the kth battery, the boundaries of its power can be defined as

$$\begin{aligned}P_{\text{ESS}}(k,t) \geq\; & P_{\text{ESS}_{\text{th2}}}(k) \\ & + c(k) * (1 - \text{status}(k,t)), \quad \forall k,t \end{aligned} \tag{13}$$

$$\begin{aligned}P_{\text{ESS}}(k,t) \leq\; & P_{\text{ESS}_{\text{th1}}}(k) \\ & + d(k) * (1 - \text{status}(k,t)), \quad \forall k,t \end{aligned} \tag{14}$$

where $Pbat_{\text{th1}}(k)$ and $Pbat_{\text{th2}}(k)$ are the boundaries values for the power in the kth battery in the case of fully charged condition, as shown in Fig. 10, and the constants $c(k)$ and $d(k)$ are

$$c(k) = \; P_{\text{ESS}_{\min}}(k) - P_{\text{ESS}_{\text{th2}}}(k) \tag{15}$$

$$d(k) = \; P_{\text{ESS}_{\max}}(k) - P_{\text{ESS}_{\text{th1}}}(k). \tag{16}$$

At the same time, it is not required to absorb energy from the dispatchable sources when the batteries are charged and the power curtailment should be allowed. Therefore, the constraints for the generation units can be written as

$$\begin{aligned}0 \leq P_g^d(i_d,t) \leq\; & \left(\frac{1}{n_k} * \sum_{k=1}^{n_k} (1 - \text{status}(k,t))\right) \\ & * P_{g_{\max}}^d(i_d,t), \quad \forall t, i_d \end{aligned} \tag{17}$$

$$\begin{aligned}0 \leq P_{\text{curt}}(i_{nd},t) \leq\; & \left(\frac{1}{n_k} * \sum_{k=1}^{n_k} \text{status}(k,t)\right) \\ & * P_{g_{\max}}^{nd}(i_{nd},t) \;\; \forall t, i_{nd} \end{aligned} \tag{18}$$

where $P_{g_{\max}}^d(i_d,t)$ and $P_{g_{\max}}^{nd}(i_{nd},t)$ are forecast datasets in terms of t in order to consider cases when the available power is variable, for instance when the source is a RES.

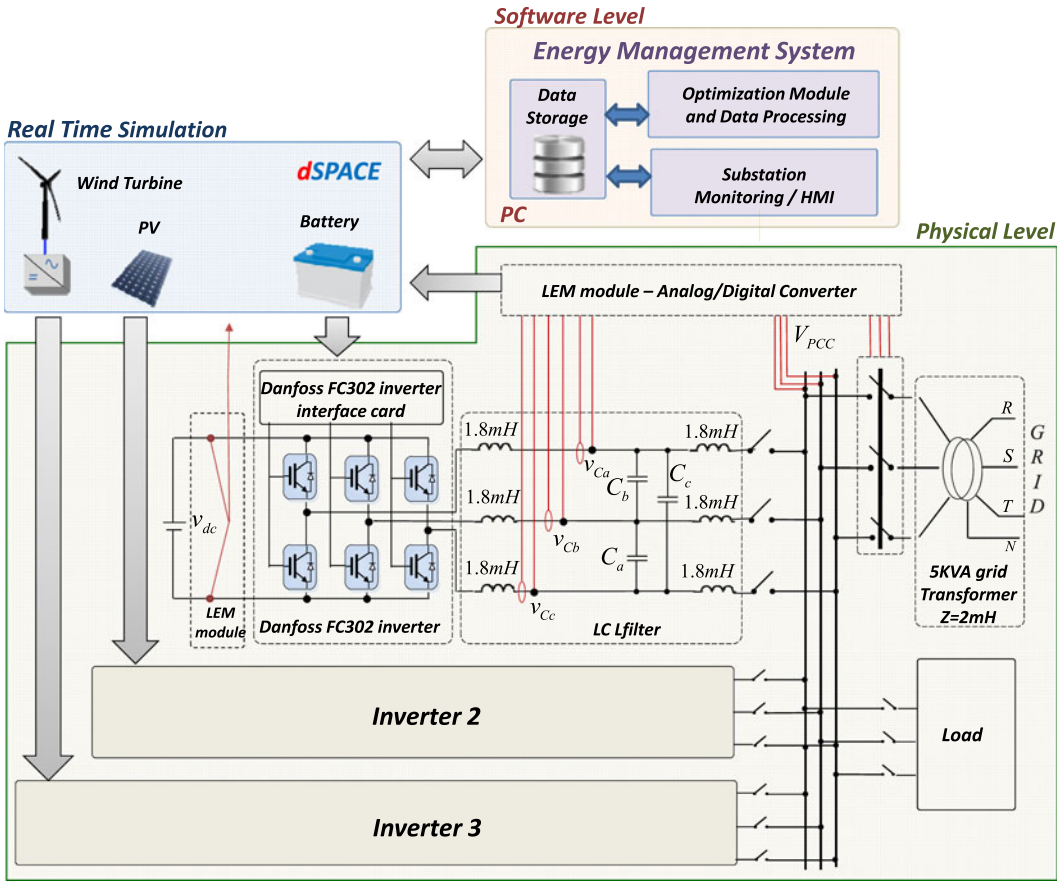

Fig. 11. Hardware in the loop implementation.

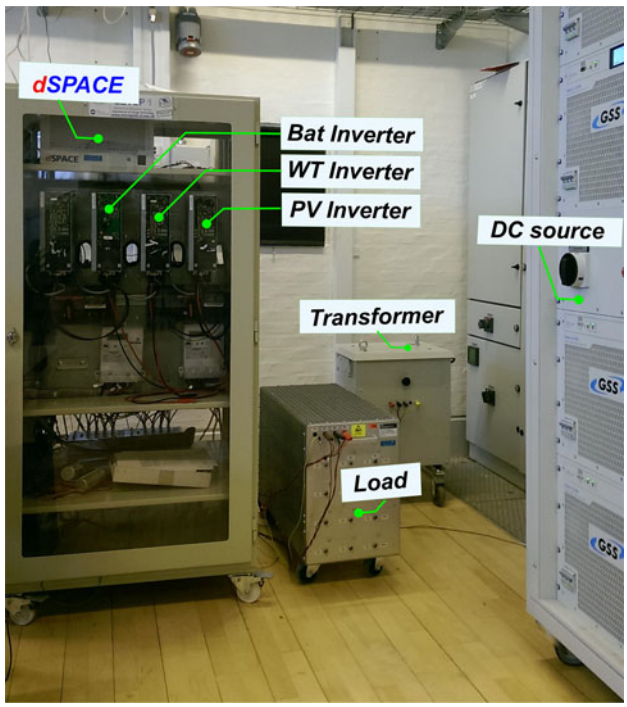

Fig. 12. Experimental setup.

TABLE IV
PARAMETERS OF THE MICROGRID

Parameter	Symbol	Value
	Power Stage	
Nominal Voltage	E^*	$230 * \sqrt{2}$ V
Nominal Frequency	ω^*	$2 * \pi * 50$ rad/s
Inverter inductors	L	1.8 mH
Filter Capacitor	C	27μF
Nominal Load	P_{Load}	600 W
Maximum (RESs) and (ESSs) Power Rating	P_{max}	± 1400 W
Reactive power Reference	Q^*	0 VAr
	Battery Array	
Nominal Voltage	V bat	672 V
Regulation Voltage	V_r	756 V
Nominal Battery Capacity	C_{bat}	16 Ah

To summarized, the boundaries of the decision variables are presented in table III and the complete model is composed by the (4–14), (17), and (18).

C. Optimization Statements for the Case Study

The selected case study is a PV-wind-battery Microgrid oriented to self-consumption operation and does not sell energy

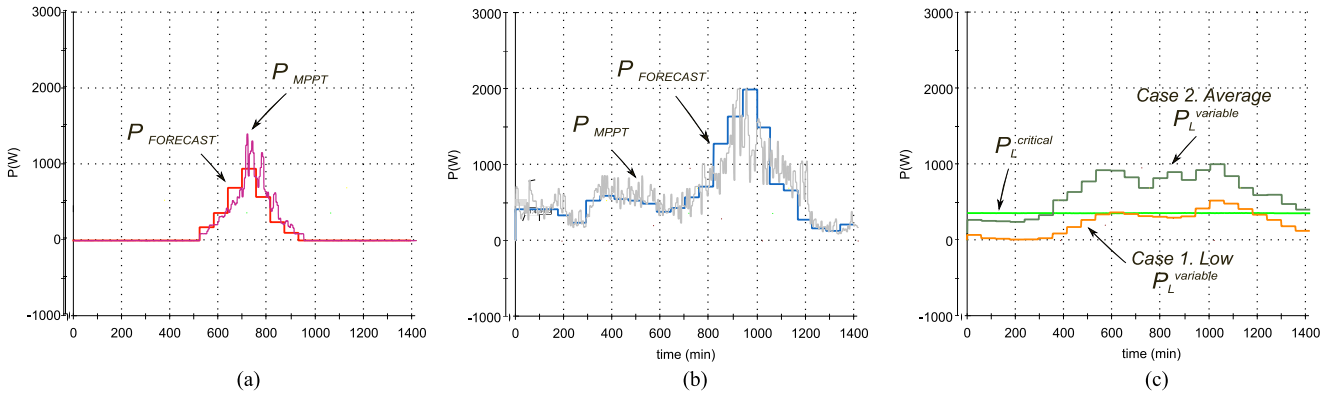

Fig. 13. Sets of input data: forecast data and P_{MPPT} generation profiles are presented in (a) and (b) for PV and WT, respectively. Demand power profiles are in (c) variable loads for case 1 and 2, and critical load.

to the grid, operating in connected islanded mode, namely, the power exchange with the utility is avoided [21].

Specifically, the power variables to be scheduled are the power of the battery ($P_{\mathrm{ESS}}(k,t)$ with $k=1$), the power absorbed from the utility, defined as a dispatchable source ($P_g^d(i_d,t)$ with $i_d=1$), and the curtailed power for the RESs, which are defined as nondispatchable sources, ($P_{\mathrm{curt}}(i_{nd},t)$ with $i_{nd}=1,2$, corresponding to the PV and the WT, respectively). The results of the scheduling are saved in the data storage of the EMS.

The supervisory control of the MG uses three datasets, the power of the battery, $P_{\mathrm{bat}}^{\mathrm{sch}}=P_{\mathrm{ESS}}(1,t)$, the power absorbed from the grid, $P_{\mathrm{grid}}^{\mathrm{sch}}=P_g^d(1,t)$, and the power references for the RESs, $[P_v^{\mathrm{sch}},P_w^{\mathrm{sch}}]=P_{g_{\max}}^{nd}(i_{nd},t)-P_{\mathrm{curt}}(i_{nd},t)$, with $i_{nd}=1,2$. The power profiles, $P_{g_{\max}}^{nd}(i_{nd},t)$, corresponds to the predicted generation of the nondispatchable sources that, in this case, are equal to the predicted power in maximum power point (MPP) for the RESs, $P_{g_{\max}}^{nd}(i_{nd},t)=[P_v^{\mathrm{forecast}},P_w^{\mathrm{forecast}}]$, with $i_{nd}=1,2$.

Regarding the objective function presented in (4), the elementary cost of buying energy to the utility, $C(i_d,t)$, is defined as a function in terms of the time with a constant value during day hours and another value during the night (see Table IV). The second term, related to the nondispatchable sources, is neglected because the operating cost of the renewable resources is virtually zero ($C(i_{nd},t)=0$), [40].

The MG used as case study includes two kinds of loads ($n_l=2$), one critical load E_L^{critical} and one variable load $E_L^{\mathrm{variable}}(t)$, considered as parameters in the model.

IV. Experimental Results

In order to validate the proposed approach, the microgrid has been implemented at the Microgrid Research Laboratory in Aalborg University [41], with and without the optimization strategy, in a HiL architecture with three different levels (see Fig. 11): software level, real time simulation, and physical level.

The software level is developed in a microgrid central computer. It corresponds to the EMS that includes scheduling module, data storage, and substation monitoring as shown in Fig. 11

TABLE V
Operating Cost for Different Cases With and Without EMS

Costs (Euros)	Case 1	Case 2
Without EMS	1.24	8.61
With EMS	1.43	6.32

where the optimization model is implemented by using the commercial software called *GAMS* [42] as *AML* and setting the *solver CPLEX* within GAMS [43]. The *substation monitoring* includes the user interface and is performed by using Matlab [44].

Meanwhile, the real time simulation is performed into a real time platform (dSPACE 1006). The model downloaded to this platform is previously established in MATLAB/Simulink and it includes the RESs generation profiles with their local controllers as well as a detailed model of a valve-regulated lead-acid (VRLA) battery that models slow and fast dynamics as presented in [45]. On top of that, the references scheduled by the EMS are downloaded as a table and are read by the simulation model every time slot of the scheduling. Furthermore, the dSPACE platform is running in real time but the time slot of the generation/consumption profiles and the scheduling have been scaled down to 60 s, so that the whole simulation spends 1440 s instead 1440 min as in [46]. Simultaneously, the capacity of the battery has been scaled in the same proportion. Namely, the real capacity of the battery Cap_{bat} can be scaled in the time base 1 h to 1 min (3600 s : 60 s) and obtain Cap_{sim} by applying the simple relation, $\mathrm{Cap}_{\mathrm{sim}}=(60/3600)*\mathrm{Cap}_{\mathrm{bat}}=\mathrm{Cap}_{\mathrm{bat}}/60$.

The physical level is integrated by three inverters fed by a stiff dc source. Each of the inverters is connected to a LCL filter which, in turn, is connected to the common bus. The experimental setup is shown in Fig. 12 and the parameters of the microgrid are summarized in Table IV.

In order to validate the performance of the proposed strategy, the power profiles for PV and WT, shown in Fig. 13(a) and (b), have been obtained based on real data of irradiance and wind speed acquired from [47], and by considering simplified power calculation models as presented in [13]. The generation

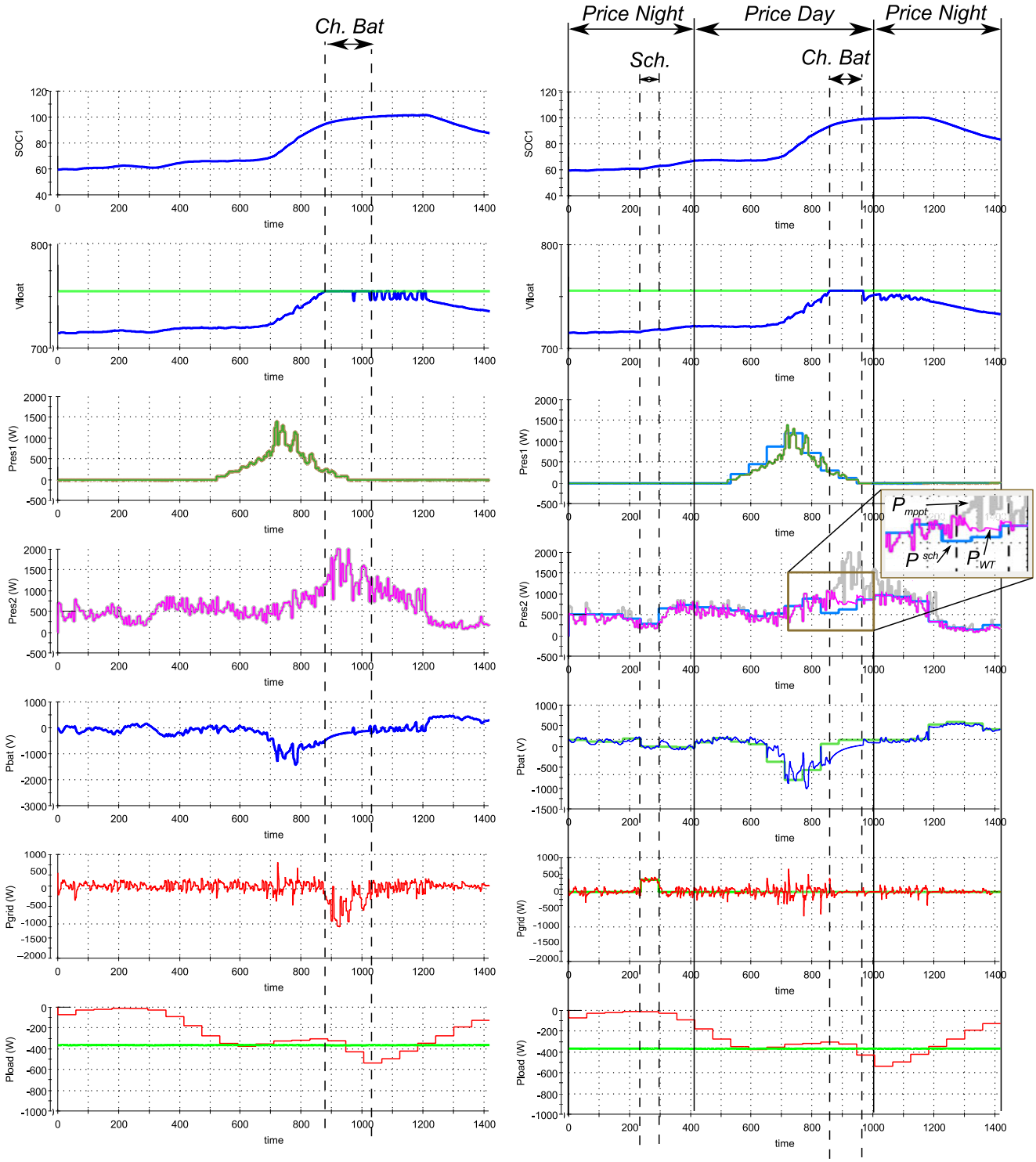

Fig. 14. Relevant measured variables of the MG without (left) and with (right) EMS in *Case 1*. Top to bottom: SoC of the battery, Battery voltage, PV power, WT power, battery power, power absorb/inject from the main grid, and consumption profiles.

profiles used in the scheduling process are presented as P_{FORECAST} in Fig. 13(a) and (b), while the experimental verification is executed by using the P_{MPPT} power profile of RESs.

With respect to the consumption, a fixed load and two profiles of variable load (weekend and weekday profiles) have been defined, as presented in Fig. 13(c). The variable profiles have been obtained from [48]. These profiles are used both in scheduling and experimental verification. They have been chosen to show how the system operates with enough local energy to supply the loads (*Case 1*) and when the MG has to absorb energy from the main grid (*Case 2*).

For scheduling and experimental verification, the initial condition of SoC is set as 60%. Additionally, the behavior of the MG is presented with and without the EMS for the two defined

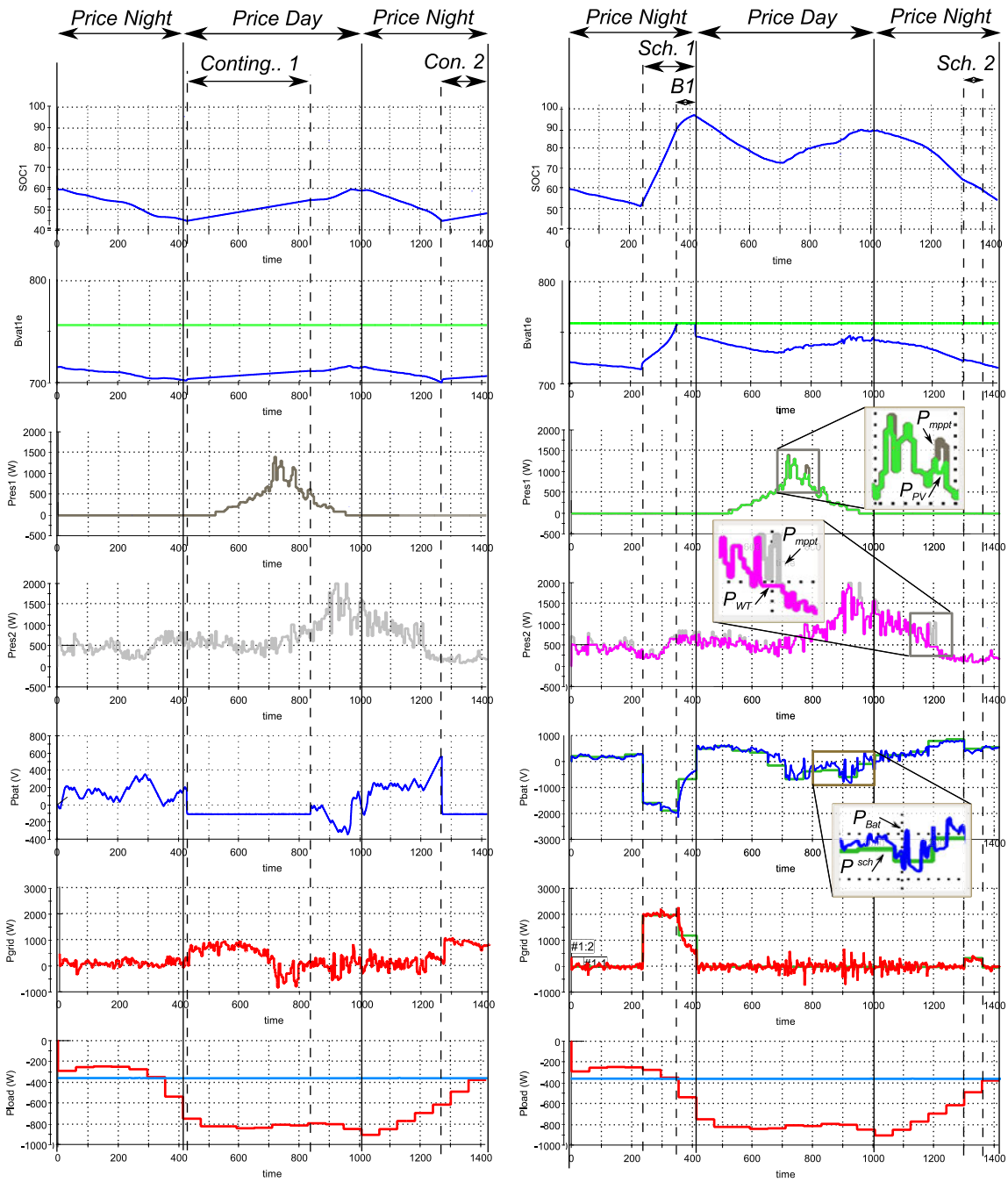

Fig. 15. Relevant measured variables of the MG without (left) and with (right) EMS in *Case 2*. Top to bottom: SoC of the battery, Battery voltage, PV power, WT power, battery power, power absorb/inject from the main grid, and consumption profiles.

variable loads. To perform the experiment without the EMS, the reference of the main grid is set as 0 kW and the RESs operate in MPPT mode. The operating costs obtained for each case are presented in Table V and they will be discussed along this section.

A. *Case 1. Low Demand Profile*

In this case, the local energy is enough to supply the load without absorbing energy from the main grid. The experimental results presented in Fig. 14 are obtained for the MG without EMS (left side) and with EMS (right side) and for each one, the variables, from top to bottom are SoC of the battery, battery voltage (with the threshold voltage), PV power, WT power, battery power, power absorbed from the main grid, and demand profiles. In the implementation without EMS, the power of the RESs correspond to the maximum available power P_{MPPT} while in the case with EMS, the results include also the reference power provided by the EMS P_{sch}, and the measured RES power P_V and P_W.

From the results obtained without EMS (left side in Fig. 14), the implemented supervisory control is able to keep the power

absorbed from the main grid about 0 kW (sixth frame) by providing references for the battery (fifth frame) as long as the battery is not fully charged which means the battery voltage (blue line in second frame) is lower than the threshold value (green line in second frame). In this case, operating cost is 1.24 euros as presented in Table V.

If the battery is charged, its control changes to grid noninteractive mode and does not follow the references provided by the supervisory control (period *Ch. Bat* in left side of Fig. 14) in order to avoid overvoltage that can damage it or reduce its lifetime, as mentioned in Section II-A2. It can be seen that, during this period, the system is not able to control the power exchanged with the main grid and the surplus energy is injected to the utility.

The results obtained by implementing the EMS (right side in Fig. 14) show that the system can follow the power profile scheduled for the main grid at any time. The EMS schedules to absorb energy from the grid in one time slot (period *Sch.* in right side of Fig. 14), when the price is low and, after that, the profile is 0 kW. The EMS also establishes the curtailment of the WT generation when the battery is charged. This reduction of the RES generation is scheduled before the battery is charged because it was expected more energy from the PV. In the highlighted box of P_{WT}, it can be seen how the supervisory control adjusts the scheduled reference P^{sch} according to the available energy P_{MPPT}. The operating cost is 1.43 euros (see Table V), which is a little higher than in the previous case since it is required to restrict some energy from RESs in order to get control over the system at any time.

B. Case 2. Average Demand Profile

In this case, the consumption is high enough to require absorbing energy from the main grid at some time of the day. The set of variables presented in Fig. 15 are similar to the one presented in *Case 1*, but in the power of RESs of the MG with EMS (third and forth frames of right side), it is shown that the maximum available power P_{MPPT} and the measured RES power P_V and P_W.

From the results obtained by implementing the MG without the EMS, it can be seen that the supervisory system is able to hold the SoC of the battery over a predefined value in order to avoid damage of the battery [15]. As explained in Section III, when the SoC is 45%, the supervisory system activates the contingency unit and sets a constant charge mode of the battery until the SoC reaches 55%, as shown in periods *Conting. 1* and *Conting. 2* in the left side of Fig. 15. Therefore, the system requires to absorb power from the main grid (sixth frame of the left side in Fig. 15), regardless if the price at this time of the day is high (*price day*) or low (*price night*). In this way, the resulting operating cost is 8.61 euros as presented in Table V. Apart from those periods, the supervisory control is able to set the power of the grid about 0 kW.

For the experimental results of the MG with the EMS shown in the right side of Fig. 15, the optimization process schedules to absorb power from the grid during the periods *Sch. 1* and *Sch. 2*, which are within the lowest cost of the grid, *Price Night* period, reducing the operational cost, which results to be 6.32 euros, as shown in Table V. In this way, the battery is charged in period $B1$ (see Fig. 15) and can manage the unbalances between RES generation and consumption during the high cost of the grid, *Price Day* period. The highlighted box of the fifth frame shows how the supervisory control adjusts the references given by the scheduling process P^{sch}. Meanwhile, the highlighted boxes related to RESs show the available power P_{MPPT} and the measured power P_{PV}, P_{WT}. The last one is the result of the downwards management of the RES energy and the regulation of the supervisory control.

In the *Case 2*, the performance of the battery without using the EMS is a reactive approach that uses the battery as much as it is required to reduce the cost without considered how high the levels of DoD can be achieved (in this case 45% twice during the time horizon) and without ensuring similar conditions for the next day. Meanwhile, all these conditions are included as constraints in the EMS, avoiding the damage of the battery and increasing its lifespan.

V. Conclusion

An energy management system has been integrated in a grid-connected hybrid microgrid. It has been implemented as a modular system in which a general generation-side optimization model has been defined to minimize the operation cost of an MG. This model has been defined in a flexible way so that it can be used for different amounts of DERs. A fuzzy-based supervisory control has been implemented in order to manage the deviation of the utility power from the predefined reference by adjusting the set-points of the DERs provided by the EMS. The theoretical assumptions were verified experimentally by implementing the MG with and without the EMS. It is possible to conclude that the EMS allows to reduce cost in the MG and also can include technical restriction for managing the storage devices in a proper way. As future work, the optimization problem can be improved by considering power losses and including demand side management programs. Additionally, this approach should be implemented in a rolling horizon scheduling so that it can be applicable without relying on very accurate prediction data. Further work regarding robust scheduling managing uncertainty is still under way.

References

[1] J. Vasquez, J. Guerrero, M. Savaghebi, J. Eloy-Garcia, and R. Teodorescu, "Modeling, analysis, and design of stationary-reference-frame droop-controlled parallel three-phase voltage source inverters," *IEEE Trans. Ind. Electron.*, vol. 60, no. 4, pp. 1271–1280, Apr. 2013.

[2] F. Nejabatkhah and Y. W. Li, "Overview of power management strategies of hybrid ac/dc microgrid," *IEEE Trans. Power Electron.*, vol. 30, no. 12, pp. 7072–7089, Dec. 2015.

[3] Q. Jiang, M. Xue, and G. Geng, "Energy management of microgrid in grid-connected and stand-alone modes," *IEEE Trans. Power Syst.*, vol. 28, no. 3, pp. 3380–3389, Aug. 2013.

[4] F. Katiraei, R. Iravani, N. Hatziargyriou, and A. Dimeas, "Microgrids management," *IEEE Power Energy Mag.*, vol. 6, no. 3, pp. 54–65, May 2008.

[5] J. de Matos, F. S. F.e Silva, and L. de S Ribeiro, "Power control in AC isolated microgrids with renewable energy sources and energy storage systems," *IEEE Trans. Ind. Electron.*, vol. 62, no. 6, pp. 3490–3498, Jun. 2015.

[6] M. Iqbal, M. Azam, M. Naeem, A. Khwaja, and A. Anpalagan, "Optimization classification, algorithms and tools for renewable energy: A review," *Renewable Sustain. Energy Rev.*, vol. 39, pp. 640–654, 2014.
[7] G. Oriti, A. L. Julian, and N. J. Peck, "Power-electronics-based energy management system with storage," *IEEE Trans. Power Electron.*, vol. 31, no. 1, pp. 452–460, Jan. 2016.
[8] G. Byeon, T. Yoon, S. M. Oh, and G. Jang, "Energy management strategy of the DC distribution system in buildings using the EV service model," *IEEE Trans. Power Electron.*, vol. 28, no. 4, pp. 1544–1554, Apr. 2013.
[9] Y. K. Chen, Y. C. Wu, C. C. Song, and Y. S. Chen, "Design and implementation of energy management system with fuzzy control for dc microgrid systems," *IEEE Trans. Power Electron.*, vol. 28, no. 4, pp. 1563–1570, Apr. 2013.
[10] W. Shi, X. Xie, C.-C. Chu, and R. Gadh, "Distributed optimal energy management in microgrids," *IEEE Trans. Smart Grid*, vol. 6, no. 3, pp. 1137–1146, May 2015.
[11] F. Marra and G. Yang, "Decentralized energy storage in residential feeders with photovoltaics," in *Energy Storage Smart Grids*, P. D. Lu, Ed. San Diego, CA, USA: Academic, 2015, pp. 277–294.
[12] P. Malysz, S. Sirouspour, and A. Emadi, "An optimal energy storage control strategy for grid-connected microgrids," *IEEE Trans. Smart Grid*, vol. 5, no. 4, pp. 1785–1796, Jul. 2014.
[13] A. H. Fathima and K. Palanisamy, "Optimization in microgrids with hybrid energy systems: A review," *Renewable Sustain. Energy Rev.*, vol. 45, pp. 431–446, 2015.
[14] Z. Zhao, "Optimal energy management for microgrids," Ph.D. dissertation, Clemson Univ., Clemson, SC, USA, 2012.
[15] I. S. C. C. 21, "Guide for optimizing the performance and life of lead-acid batteries in remote hybrid power systems," *IEEE Standard 1561–2007*, 2008, pp. C1–25.
[16] T. Strasser "A review of architectures and concepts for intelligence in future electric energy systems," *IEEE Trans. Ind. Electron.*, vol. 62, no. 4, pp. 2424–2438, Apr. 2015.
[17] H. Beltran, E. Bilbao, E. Belenguer, I. Etxeberria-Otadui, and P. Rodriguez, "Evaluation of storage energy requirements for constant production in PV power plants," *IEEE Trans. Ind. Electron.*, vol. 60, no. 3, pp. 1225–1234, Mar. 2013.
[18] A. Hooshmand, B. Asghari, and R. Sharma, "Experimental demonstration of a tiered power management system for economic operation of grid-tied microgrids," *IEEE Trans. Sustain. Energy*, vol. 5, no. 4, pp. 1319–1327, Oct. 2014.
[19] M. Castillo-Cagigal "PV self-consumption optimization with storage and active DSM for the residential sector," *Solar Energy*, vol. 85, no. 9, pp. 2338–2348, 2011.
[20] A. Sangwongwanich, Y. Yang, and F. Blaabjerg, "High-performance constant power generation in grid-connected PV systems," *IEEE Trans. Power Electron.*, vol. 31, no. 3, pp. 1822–1825, 2016.
[21] P. A. Ostergaard, "Reviewing optimisation criteria for energy systems analyses of renewable energy integration," *Energy*, vol. 34, no. 9, pp. 1236–1245, 2009.
[22] C. Li "Comprehensive review of renewable energy curtailment and avoidance: A specific example in china," *Renewable Sustain. Energy Rev.*, vol. 41, pp. 1067–1079, 2015.
[23] A. Sobu and G. Wu, "Dynamic optimal schedule management method for microgrid system considering forecast errors of renewable power generations," in *Proc. IEEE Int. Conf., Power Syst. Technol.*, Oct. 2012, pp. 1–6.
[24] *Microgrid technology research and demonstration. Aalborg University*, (2015, Oct.). [Online]. Available: www.meter.et.aau.dk
[25] J. Rocabert, A. Luna, F. Blaabjerg, and P. Rodriguez, "Control of power converters in AC microgrids," *IEEE Trans. Power Electron.*, vol. 27, no. 11, pp. 4734–4749, Nov. 2012.
[26] D. Wu, F. Tang, T. Dragicevic, J. Vasquez, and J. Guerrero, "Autonomous active power control for islanded AC microgrids with photovoltaic generation and energy storage system," *IEEE Trans. Energy Convers.*, vol. 29, no. 4, pp. 882–892, Dec. 2014.
[27] D. Wu, F. Tang, T. Dragicevic, J. Vasquez, and J. Guerrero, "Coordinated primary and secondary control with frequency-bus-signaling for distributed generation and storage in islanded microgrids," in *Proc. IEEE 39th Annu. Conf. Ind. Electron. Soc.*, Nov. 2013, pp. 7140–7145.
[28] W. Yan, Z. Shu-Zhen, H. Cheng, and R. Jiang-jun, "Dynamic model and control of voltage source converter based HVDC," in *Proc. Asia-Pacific Power Energy Eng. Conf.*, Mar. 2009, pp. 1–5.
[29] A. Dizqah, A. Maheri, K. Busawon, and A. Kamjoo, "A multivariable optimal energy management strategy for standalone DC microgrids," *IEEE Trans. Power Syst.*, vol. 30, no. 5, pp. 2278–2287, Sep. 2015.
[30] V. Salas, E. Olías, A. Barrado, and A. Lázaro, "Review of the maximum power point tracking algorithms for stand-alone photovoltaic systems," *Solar Energy Mater. Solar Cells*, vol. 90, no. 11, pp. 1555–1578, 2006.
[31] C. Patsios, A. Chaniotis, M. Rotas, and A. Kladas, "A comparison of maximum-power-point tracking control techniques for low-power variable-speed wind generators," in *Proc. 8th Int. Symp. Adv. Electromech. Motion Syst. Elect. Drives Joint Symp.*, Jul. 2009, pp. 1–6.
[32] D. Linden and T. Reddy, *Handbook of Batteries*. New York, NY, USA: McGraw-Hill, 2002.
[33] N. L. Diaz, T. Dragicevic, J. Vasquez, and J. Guerrero, "Intelligent distributed generation and storage units for DC microgrids: A new concept on cooperative control without communications beyond droop control," *IEEE Trans. Smart Grid*, vol. 5, no. 5, pp. 2476–2485, Sep. 2014.
[34] T. Dragicevic, J. Guerrero, J. Vasquez, and D. Skrlec, "Supervisory control of an adaptive-droop regulated DC microgrid with battery management capability," *IEEE Trans. Power Electron.*, vol. 29, no. 2, pp. 695–706, Feb. 2014.
[35] A. Luna, N. Diaz, F. Andrade, M. Graells, J. Guerrero, and J. Vasquez, "Economic power dispatch of distributed generators in a grid-connected microgrid," in *Proc. 9th Int. Conf. Power Electron. ECCE Asia*, Jun. 2015, pp. 1161–1168.
[36] D. Tenfen and E. C. Finardi, "A mixed integer linear programming model for the energy management problem of microgrids," *Elect. Power Syst. Res.*, vol. 122, pp. 19–28, 2015. [Online]. Available: http://www.sciencedirect.com/science/article/pii/S0378779614004659
[37] R. Bosch and M. Trick, "Integer programming," in *Search Methodologies*, E. Burke and G. Kendall, Eds. Berlin, Germany: Springer 2005, pp. 69–95. [Online]. Available: http://dx.doi.org/10.1007/0-387-28356-0_3
[38] C. Monteiro, "Overview of electric power generation systems," in *Electric Power Systems: Advanced Forecasting Techniques Optimal Generation Scheduling*, J. P. S. Catalao Ed. Boca Raton, FL, USA: CRC Press, 2015, ch. 1.
[39] K. Shimomachi, R. Hara, H. Kita, M. Noritake, H. Hoshi, and K. Hirose, "Development of energy management system for DC microgrid for office building: Day ahead operation scheduling considering weather scenarios," in *Proc. Power Syst. Comput. Conf.*, Aug 2014, pp. 1–6.
[40] G. B. Shrestha and S. Qiao, "Price-based scheduling for gencos," in *Electric Power Systems: Advanced Forecasting Techniques Optimal Generation Scheduling*, J. P. S. Catalao, Ed. Boca Raton, FL, USA: CRC Press, 2015, ch. 6.
[41] *Intelligent microgrid laboratory. Aalborg University* [Online]. Available: http://www.et.aau.dk/department/laboratory-facilities/intelligent-microgrid-lab/
[42] *G. D. Corporation. General algebraic modeling system (GAMS) release 24.2.1*, (2013). [Online]. Available: http://www.gams.com/
[43] *GAMS development corporation GAMS - The Solvers Manual.*, (2016, Mar.). [Online]. Available: http://www.gams.com/help/topic/gams.doc/solvers/allsolvers.pdf
[44] MATLAB, "version 8.0.0.783 (r2012b)," Natick, MA, USA, 2012.
[45] T. Kim and W. Qiao, "A hybrid battery model capable of capturing dynamic circuit characteristics and nonlinear capacity effects," *IEEE Trans. Energy Convers.*, vol. 26, no. 4, pp. 1172–1180, Dec. 2011.
[46] A. Ruiz-Alvarez, A. Colet-Subirachs, F. Alvarez-Cuevas Figuerola, O. Gomis-Bellmunt, and A. Sudria-Andreu, "Operation of a utility connected microgrid using an IEC 61850-based multi-level management system," *IEEE Trans. Smart Grid*, vol. 3, no. 2, pp. 858–865, Jun. 2012.
[47] *Photovoltaic system. Aalborg Univ.*, (2015, Oct.). [Online]. Available: http://www.et.aau.dk/research-programmes/photovoltaic-systems
[48] *Nord pool spot*, (2016, Feb.). [Online]. Available: http://www.nordpoolspot.com/download-center/

Adriana Luna (S'06) received the B.S. degree in electronic engineering, in 2006 and the M.S. degree in industrial automation in 2011, both from Universidad Nacional de Colombia, Bogot, Colombia. She is currently working toward the Ph.D degree in the Department of Energy Technology, Aalborg University, Aalborg, Denmark, as part of the Denmark Microgrids Research Programme (www.microgrids.et.aau.dk).

Her research interests include energy management systems of microgrids, and specifically on architectures and algorithms for scheduling and optimization for operation level in microgrids.

Nelson Diaz (S'09) received the B.S degree in electronic engineering from the Universidad Distrital Francisco Jose de Caldas (F.J.C.), Chapinero, Colombia, in 2008, and the M.S. degree in industrial automation from the Universidad Nacional de Colombia, Bogota, Colombia, in 2011. He is currently working toward the Ph.D. degree at the Department of Energy Technology, Aalborg University, Aalborg, Denmark.

He is a Member of the Research Laboratory of Alternative Energy Sources, Universidad Distrital F.J.C., and Microgrid Research Group, Aalborg University. His current research interests include microgrids and power converters control.

Moisès Graells received the Bachelor's degree in chemical science from the Universitat Autónoma de Barcelona (UAB), Barcelona, Spain, in 1989, and the Ph.D. degree in process systems engineering from Universitat Politécnica de Catalunya (UPC), Barcelona, Spain, in 1996.

He is currently an Associate Professor of chemical engineering at UPC, Barcelona, Spain. His research interests include the modeling, integration, and optimization of chemical processes, especially batch processes. Regarding methodological aspects, his interests are the modeling and optimization techniques, computer aided tools for decision making, information management, and standardization. Recently, his investigation also includes the modeling of complex chemical systems and the study of renewable energy systems.

Juan C. Vasquez (M'12–SM'14) received the B.S. degree in electronics engineering from the Autonomous University of Manizales, Manizales, Colombia, and the Ph.D. degree in automatic control, robotics, and computer vision from the Technical University of Catalonia, Barcelona, Spain, in 2004 and 2009, respectively.

He was with the Autonomous University of Manizales working as a Teaching Assistant and the Technical University of Catalonia as a Postdoctoral Assistant in 2005 and 2008, respectively. In 2011, he was an Assistant Professor and from 2014, he is working as an Associate Professor at the Department of Energy Technology, Aalborg University, Denmark, where he is the Vice-Programme Leader of the Microgrids Research Program. From February 2015 to April. 2015, he was a Visiting Scholar at the Center of Power Electronics Systems at Virginia Tech. His current research interests include operation, advanced hierarchical and cooperative control, optimization, and energy management applied to distributed generation in ac and dc microgrids. He has authored and coauthored more than 100 technical papers only in Microgrids in international IEEE conferences and journals.

Dr. Vasquez is currently a Member of the IEC System Evaluation Group SEG4 on LVDC Distribution and Safety for use in Developed and Developing Economies, the Renewable Energy Systems Technical Committee TC-RES in IEEE Industrial Electronics, Power electronics society, Industry applications society, and Power and energy societies.

Josep M. Guerrero (S'01–M'04–SM'08–F'15) received the B.S. degree in telecommunications engineering, the M.S. degree in electronics engineering, and the Ph.D. degree in power electronics from the Technical University of Catalonia, Barcelona, in 1997, 2000, and 2003, respectively.

Since 2011, he has been a Full Professor with the Department of Energy Technology, Aalborg University, Denmark, where he is responsible for the Microgrid Research Program. From 2012, he is a Guest Professor at the Chinese Academy of Science and the Nanjing University of Aeronautics and Astronautics; from 2014, he is the Chair Professor in Shandong University; from 2015, he is a Distinguished Guest Professor in Hunan University; and from 2016, he is a Visiting Professor Fellow at Aston University, U.K. His research interests include different microgrid aspects, including power electronics, distributed energy-storage systems, hierarchical and cooperative control, energy management systems, smart metering and the internet of things for ac/dc microgrid clusters, and islanded minigrids; recently especially focused on maritime microgrids for electrical ships, vessels, ferries, and seaports.

Prof. Guerrero is an Associate Editor for the IEEE TRANSACTIONS ON POWER ELECTRONICS, the IEEE TRANSACTIONS ON INDUSTRIAL ELECTRONICS, and the IEEE INDUSTRIAL ELECTRONICS MAGAZINE, and an Editor for the IEEE TRANSACTIONS ON SMART GRID, and IEEE TRANSACTIONS ON ENERGY CONVERSION. He has been a Guest Editor of the IEEE TRANSACTIONS ON POWER ELECTRONICS Special Issues: Power Electronics for Wind Energy Conversion and Power Electronics for Microgrids; the IEEE TRANSACTIONS ON INDUSTRIAL ELECTRONICS Special Sections: Uninterruptible Power Supplies systems, Renewable Energy Systems, Distributed Generation and Microgrids, and Industrial Applications and Implementation Issues of the Kalman Filter; the IEEE TRANSACTIONS ON SMART GRID Special Issues: Smart DC Distribution Systems and Power Quality in Smart Grids; the IEEE TRANSACTIONS ON ENERGY CONVERSION Special Issue on Energy Conversion in Next-generation Electric Ships. He was the Chair of the Renewable Energy Systems Technical Committee of the IEEE Industrial Electronics Society. He received the Best Paper Award of the IEEE TRANSACTIONS ON ENERGY CONVERSION for the period 2014–2015. In 2014 and 2015, he was awarded by Thomson Reuters as Highly Cited Researcher, and in 2015 he was elevated as IEEE Fellow for his contributions on distributed power systems and microgrids.